



Cite this: DOI: 10.1039/d5ay00516g

An electrochemical green PC/IL@GCE sensor for trace-level detection of hazardous triclopyr herbicide in serum and fruits†

Puja Tomar, Nimisha Jadon * and Swati Shrivastava 

The present work reports a green approach for the development of a new electrochemical sensor based on a pectin and ionic liquid composite (PC/IL) for sensitive detection of triclopyr (TCP), which is a useful pesticide. The fabricated sensor was characterized using microscopic (Scanning Electron Microscopy (SEM)), spectroscopic (Energy Dispersive X-ray (EDX) spectroscopy, ultraviolet-visible (UV-vis) spectroscopy, X-ray diffraction (XRD), Fourier Transform Infrared (FTIR) spectroscopy, Electrochemical Impedance Spectroscopy (EIS)), and cyclic voltammetric methods. The sensor displayed a large surface area, high conductivity, and rich porosity, which contributed to achieving high electrochemical performances toward sensing applications. Experimental parameters, including pH, solvent, concentration, frequency, and amplitude, were optimized for the detection of TCP at PC/IL@GCE using voltammetric techniques. The developed sensor exhibited high sensitivity, selectivity and reproducibility for TCP detection with the detection limit (LOD) and quantification limit (LOQ) as low as 223 pg mL⁻¹ and 745 pg mL⁻¹, respectively. The electrode also exhibited satisfactory recovery in the range of 99.64–101.92%, 99.44–100.87%, and 99.02–101.40% for the detection of TCP in real samples of human serum, tomato, and apple, respectively. Additionally, the environmental sustainability of the developed sensor was assessed, demonstrating a 92% greener aspect.

Received 27th March 2025
Accepted 26th May 2025DOI: 10.1039/d5ay00516g
rsc.li/methods

1. Introduction

In modern agriculture, pesticides play a significant role in healthy crop production without compromising the yield. They include a wide variety of chemical agents, such as insecticides, nematicides, weedicides, rodenticides, fungicides, and herbicides, which are used to eliminate different pests, protect crops from damage, and ensure higher production levels. Among the diverse array of pesticides, triclopyr (TCP), commonly known as triclopyr acid, refers to the agrochemical active substance 3,5,6-trichloro-2-pyridyloxyacetic acid and has been used as a herbicide since 1979.¹ In commercial products, TCP is also available as triclopyr butoxyethyl ester (T-BEE) and triclopyr triethylamine salt (T-TEA).² These forms, including the acidic form, are globally registered for controlling broadleaf weeds and woody plants. After pesticides are sprayed, they accumulate in soil and water, posing significant risks to animals, humans, and the environment. The average half-life of triclopyr acid in soil is around 30 days. In water, the salt formulation is soluble and may degrade within hours under sunlight, while the non-water-soluble ester can take longer to break down. Both salt and ester

formulations are relatively less toxic to mammals, but the ester can be highly toxic to fish and aquatic organisms.^{3,4}

Since TCP is applied directly to water for aquatic weed treatment, its non-water-soluble ester may pose a risk to aquatic life. Regulating agencies such as the Environmental Protection Agency (EPA), Water Framework Directives (WFD) (2000/60/EC) establish low limits of permissible pesticide residues as well as encourage the development of analytical methods showing lower detection limits.^{5,6} There are a few analytical methods for the quantification of TCP, including immunoaffinity chromatography,⁷ fluorescent sensors,⁸ plasmonic sensors,⁹ and electrochemical methods.^{10,11} Among them, electrochemical methods showed high sensitivity and selectivity for the trace analysis of TCP. Although other methods can also accurately detect pesticides at trace levels, those techniques are time consuming and require expensive, sophisticated instrumentation and highly skilled personnel, which restrict their use in routine analysis. Therefore, a novel technique for the determination of TCP is needed. The electrochemical method effectively detects pesticides with high sensitivity and selectivity, offers simple and cost-effective analysis, and now allows for on-site testing, making it suitable for use in various environments.^{12–17}

Nowadays, green materials represent an intriguing and cost-effective class of nanomaterials that enhance the sensitivity of electrochemical sensors while also reducing their environmental impact, representing a significant shift towards a more sustainable approach.^{18,19} Among the emerging green materials,

School of Studies in Environmental Chemistry, Jiwaji University, Gwalior 474011, India. E-mail: nimisha09@yahoo.com

† Electronic supplementary information (ESI) available. See DOI: <https://doi.org/10.1039/d5ay00516g>

polysaccharides like chitosan, cellulose, and pectin are gaining significant attention for their roles in developing sustainable sensors. Pectin, in particular, stands out as a promising candidate for forming supramolecular polymer composites, due to its unique ability to interact with a broad range of organic and inorganic substances through various molecular interactions.²⁰ This versatility is enabled by pectin's molecular structure, which contains hydroxyl and carboxyl groups per repeating unit, facilitating multiple hydrogen bonds.^{21,22} In earlier applications for analyzing biomolecules, pectin-modified electrochemical sensors offer outstanding sensitivity for single and multiple analytes, quick response times, and a cost-effective method.²³

Furthermore, ionic liquids (ILs) are considered relatively eco-friendly due to their thermal stability and non-volatility at room temperature, which minimizes atmospheric release.^{14,24,25} ILs have been extensively used in sensor applications, particularly in combination with nanostructures, given their capacity to dissolve organic, inorganic, and organometallic compounds. When paired with various materials, such as silica, carbon nanomaterials, zeolites, aluminum hydroxide, and metal-organic frameworks (MOFs), ILs enhance the performance of electrochemical sensors.^{26–30} Thanks to the remarkable dissolution properties of ILs, they have been extensively used in conjunction with a wide variety of nanomaterials to enhance the sensitivity of electrochemical sensors. However, to our knowledge, the application of an ionic liquid-pectin composite in electrochemical sensors remains unexplored. In this study, we have developed a PC/IL@GCE electrochemical sensor for detecting TCP, which demonstrates excellent electrocatalytic activity, highlighting a promising green approach to electrochemical sensing. This study shows the greener approach to electrochemical sensing in comparison with non-green methods, which is confirmed by AGREE software.

2. Experimental

2.1. Chemicals

Chemicals used in the present work were used without any additional purification and were of analytical grade. Pectin powder, produced from citrus peel ($\geq 74.0\%$), was obtained from Sigma-Aldrich. Triclopyr and an ionic liquid (1-butyl-2,3-dimethylimidazolium hexafluorophosphate) of purity $>97.0\%$ were purchased from Tokyo Chemical Industry. The buffer that was utilized was Britton–Robinson buffer (BR buffer), which was prepared by using phosphoric acid ($\geq 99.0\%$), acetic acid ($\geq 99.7\%$), boric acid ($\geq 99.0\%$), and NaOH (98–100.5%). High purity water was obtained from a Millipore Milli-Q Plus system (Milford, MA, USA), and all solutions were prepared in it. Triclopyr stock solution was prepared in ethanol ($\geq 99.9\%$) that was purchased from Sigma-Aldrich. Synthetic serum samples used in analysis were also purchased from Sigma-Aldrich.

2.2. Apparatus

Electrochemical measurements were performed using an AUTOLAB 112 potentiostat/galvanostat 302N (The Netherlands) using NOVA 1.10 software. Ag/AgCl (3.0 mol per L KCl) was used

as a reference electrode; PC/IL@GCE was employed as a working electrode and a platinum wire as an auxiliary electrode. The morphological characteristics of electrodes were studied by scanning electron microscopy using a JSM 6510LV JEOL instrument. All the pH measurements were carried out with a ComSys Technologies Auto digital pH meter. All the solutions examined by electrochemical techniques were purged for 10 min with purified nitrogen gas prior to analysis. A Rigaku MiniFlex 600 was employed for X-ray diffraction, a PerkinElmer Spectrum II was used for FTIR, and a Shimadzu SALD-2300 (wing SALD II: version 3.1.1) was employed for particle size analysis; AGREE software were used for green analysis.

2.3. Fabrication of the PC/IL@GCE sensor

First, GCE was polished with alumina slurry of varying particle sizes ranging from 0.05 to 1.0 μm sequentially until a mirror-like finish was obtained. It was followed by ultrasonication in absolute ethanol and ultrapure water. GCE was further rinsed with ultrapure water and dried under a stream of nitrogen gas. For fabricating the sensor, pectin and the ionic liquid in a 1 : 1 ratio were dissolved in DMF separately, followed by sonication for 2 h. Then, the resulting solution was used to make a homogeneous suspension in a 3 : 1 ratio mixture of PC and IL and stored at 5 $^{\circ}\text{C}$ for later use. A measured volume of 5.0 μL of this suspension was then dropped onto the surface of precleaned GCE using a micropipette. The modified PC/IL@GCE was then allowed to dry naturally at room temperature for further use.

2.4. Preparation of real samples

Tomato and apple were purchased from the local market of Gwalior, Madhya Pradesh, India, for sample preparation. They were crushed separately, then 1.0 g of each was measured and dissolved individually with 10 mL of ethanol and 1.0 mM of TCP *via* ultrasonication for 1 h followed by centrifugation. Then, each prepared solution of tomato and apple was filtered with Whatman (110 mm) filter paper and transferred into a 25 mL volumetric flask separately and diluted with distilled water up to the mark. Pesticide present in soil and water poses significant risks to humans. The serum sample was also used for the analysis.³ Similarly, a stock of human serum sample was also prepared by mixing 3.6 mL of synthetic serum sample with 1.0 mL of 1.0 mM TCP, then it was vortexed and precipitated with 5.4 mL of acetonitrile. The obtained solution was centrifuged at 5000 rpm for 20 min followed by separation of the supernatant from the precipitates. The standard addition method was applied for the analysis of spiked tomato, apple, and human serum samples. The concentration was spiked up to 10, 20, 40, 80, 160 ng mL^{-1} for all samples. Square wave voltammetry and differential pulse voltammetry were used to evaluate the sensitivity of the PC/IL@GCE sensor in real samples.

3. Results and discussion

3.1. Microscopic examination of the fabricated sensor

Scanning electron microscopy (SEM) was employed to examine the structural and morphological characteristics of the PC, IL,

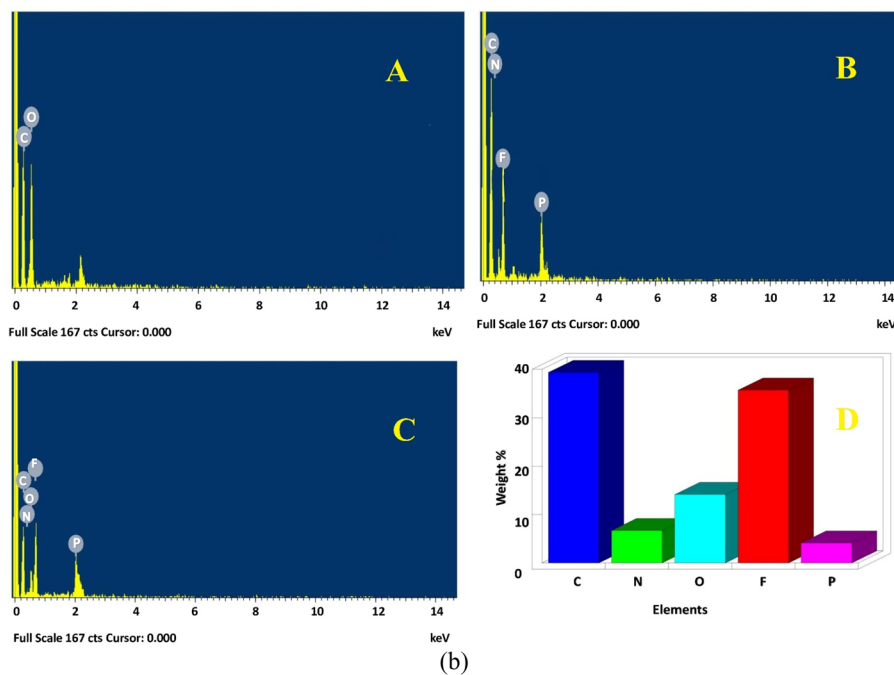
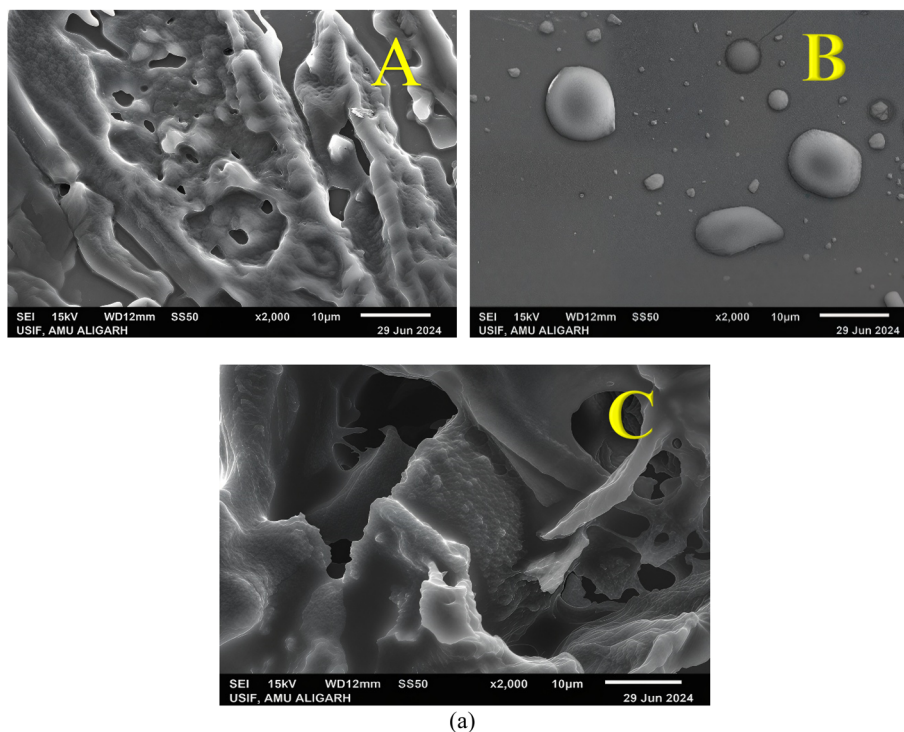


Fig. 1 (a) SEM micrographs of (A) PC, (B) IL, and (C) PC/IL; (b) EDX spectra of (A) PC, (B) IL, and (C) PC/IL and (D) bar chart for weight (%) of elements present in PC/IL.

and PC/IL composite. Figure (Fig. 1a(A)), representing the PC, reveals a homogeneous distribution of amorphous and layered, fibrous structures with small pores. Fig. (1a(B)) shows the IL with an irregular, clustered distribution of agglomerated particles, resulting in a roughened surface with embedded pores. Fig. 1a(C) illustrates the PC/IL composite, where increases in

cavities were observed due to the incorporation of the IL into the PC matrix. The presence of cavities in the SEM micrographs highlights the porosity, permeability, and surface area of the fabricated sensors. The increased porosity of the PC structure enhances permeability and provides a larger surface area in the PC/IL composite, potentially improving analyte binding

capacity and sensor performance. The PC/IL composite was consist of hydroxyl and carboxylic groups enables it to bind the sample with the sensor surface by van der Waals forces and electrostatic interaction, which makes the composite binding a reversible process.³¹ All micrographs were taken at a 10 μm scale. Additionally, particle size analysis confirmed that the average particle size of the PC/IL composite was approximately 5 μm ; $x_c = 4.72 \mu\text{m}$ in the Gaussian curve, shown in the ESI 1,[†] confirms the size of PC/IL particles.

3.2. Spectroscopic characterization of the prepared composite

The prepared PC/IL composite was examined by various spectroscopic techniques, the results of which were found to be in good agreement with their reported values. The chemical compositions of the fabricated electrodes were analyzed using the Energy Dispersive X-ray (EDX) technique, as shown in Fig. 1b(A–D). The EDX spectrum of pectin (PC) revealed the presence of carbon (C) and oxygen (O) (Fig. 1b(A)). In contrast, the spectrum of the ionic liquid (IL) indicated the presence of carbon (C), nitrogen (N), fluorine (F), and phosphorus (P) (Fig. 1b(B)). The spectrum of Fig. 1b(C) confirms that all elements carbon, oxygen, nitrogen, fluorine, and phosphorus of both PC and IL are present in the PC/IL composite, with no impurities detected. Additionally, Fig. 1b(D) displays the weight percentages of the elements present in the PC/IL composite.

Furthermore, the UV-visible spectrum (PC/IL) showed a maximum absorption at 280 nm (Fig. 2A). It usually indicates the presence of aromatic amino acids, especially protein or peptide. These amino acids possess aromatic rings that absorb light at approximately 280 nm.³² This confirms the presence of an aromatic structure in our composite used for fabrication. The peaks in the UV-visible spectra of IL, PC, and PC/IL are found to be moved from 260 nm to 280 nm, showing a shift more towards the visible range. This involves increased π - π transition, enhanced electronic transition, and so enhanced conductance. Moreover, XRD the spectrum of the PC/IL composite is presented in Fig. 2B, which confirmed its crystal-line structure. For pectin, sharp peaks are observed at $2\theta = 18.69^\circ$, 24.46° , and 25.01° , and for the IL prominent peaks are observed at $2\theta = 12.15^\circ$, 16.98° , and 22.63° when scanned at a rate of 10.00° per min at 40 kV. However, the sharp peaks at $2\theta = 11.73^\circ$, 18.86° , and 25.24° further verify the increased crystallinity of the PC/IL composite, as shown in Fig. 2B.

To investigate the intermolecular interactions among PC and IL, Fourier transform infrared (FTIR) spectroscopy was used ESI 2[†] shows the FTIR spectral analysis of pectin, ionic liquid and PC/IL composite films. For clarity, FTIR absorption peaks (wave number (cm^{-1})) and their corresponding functional groups in PC, IL, and the PC/IL composite are given in ST 1. The spectra of the pectin and ionic liquid composite exhibited more intense peaks at 3339 and 1730 cm^{-1} as compared to pectin and the ionic liquid individually, proving the enhanced interaction among PC and the IL in the PC/IL composite film. Enhanced intensity represents that crosslinking occurred effectively due to

the electrostatic interaction between PC and IL, which improved the adsorption of the analyte to the electrode surface.³³

3.3. Electrochemical characterization of the PC/IL@GCE sensor

To investigate the electrochemical nature of the modified electrodes, electrochemical impedance spectroscopy (EIS) was employed using a 3.0 mM $\text{K}_3[\text{Fe}(\text{CN})_6]$ solution in 1.0 M KCl. The Nyquist plots of the modified and bare GC electrodes included both linear and semicircular portions (Fig. 2C). The linear part corresponded to the diffusion process at lower frequencies, while the semicircular portion (at higher frequencies) was related to the charge transfer resistance (R_{ct}). The obtained results showed that the electrocatalytic activity of the modified PC/IL@GCE increased due to the decrease in R_{ct} at the surface of the sensor. The R_{ct} values obtained for bare GCE, IL@GCE, PC@GCE, and PC/IL@GCE were 100.6 Ω , 97.5 Ω , 85.8 Ω , and 39.1 Ω , respectively. The lower R_{ct} value of the developed sensor explains their good electrical conductivity and higher electrocatalytic properties, which can be attributed to the presence of a highly conductive ionic liquid and pectin on the GCE surface, which enhanced the conductivity of the interface by decreasing the interfacial resistance and thus provided a greater surface area for reaction on the modified electrode. Furthermore, the electron transfer rate constant (k_{app}) was calculated using the equation given below.

$$K_{\text{app}} = RT/F^2 R_{\text{ct}} C \quad (\text{i})$$

where R , T , F , R_{ct} and C are the gas constant (8.314 $\text{J mol}^{-1} \text{K}^{-1}$), absolute temperature of the system (298 K), Faraday constant (96 485 C mol^{-1}), charge transfer resistance and concentration of $\text{K}_3[\text{Fe}(\text{CN})_6]$ ($C = 1.0 \times 10^{-3} \text{ mol cm}^{-3}$), respectively. The obtained k_{app} values for the bare electrode, IL@GCE, PC@GCE and PC/IL@GCE are 2.6×10^{-6} , 2.7×10^{-6} , 3.1×10^{-6} and 6.8×10^{-6} , respectively. The higher k_{app} of PC/IL@GCE than the PC@GCE and bare GCE electrode indicates a faster electron transfer process of $\text{K}_3[\text{Fe}(\text{CN})_6]$ on the developed electrode surface.

Moreover, the electrochemical performance of the developed sensors was further investigated by Cyclic Voltammetry (CV) using 1.0 mM $\text{K}_3[\text{Fe}(\text{CN})_6]$ as a model redox probe. Voltammograms were recorded in a 1.0 mM $\text{K}_3[\text{Fe}(\text{CN})_6]$ solution containing 0.1 M KCl at a scan rate of 100 mV s^{-1} (Fig. 2D). The obtained results indicate that PC/IL@GCE exhibited better conductivity, and due to its improved electrocatalytic activity, it was used for further investigation. The effective surface area of the developed electrodes was also calculated based on the Randles–Sevcik equation (eqn (ii)):

$$I = (2.69 \times 10^5) ACD^{1/2} n^{3/2} \nu^{1/2} \quad (\text{ii})$$

where I signifies the anodic peak current, A represents the effective surface area of the electrode in cm^2 , C (mol cm^{-3}) denotes the concentration of the analyte, D is the analyte's diffusion coefficient, ν is the scan rate (V s^{-1}), and n is the number of electrons participating in the electrode reaction. For

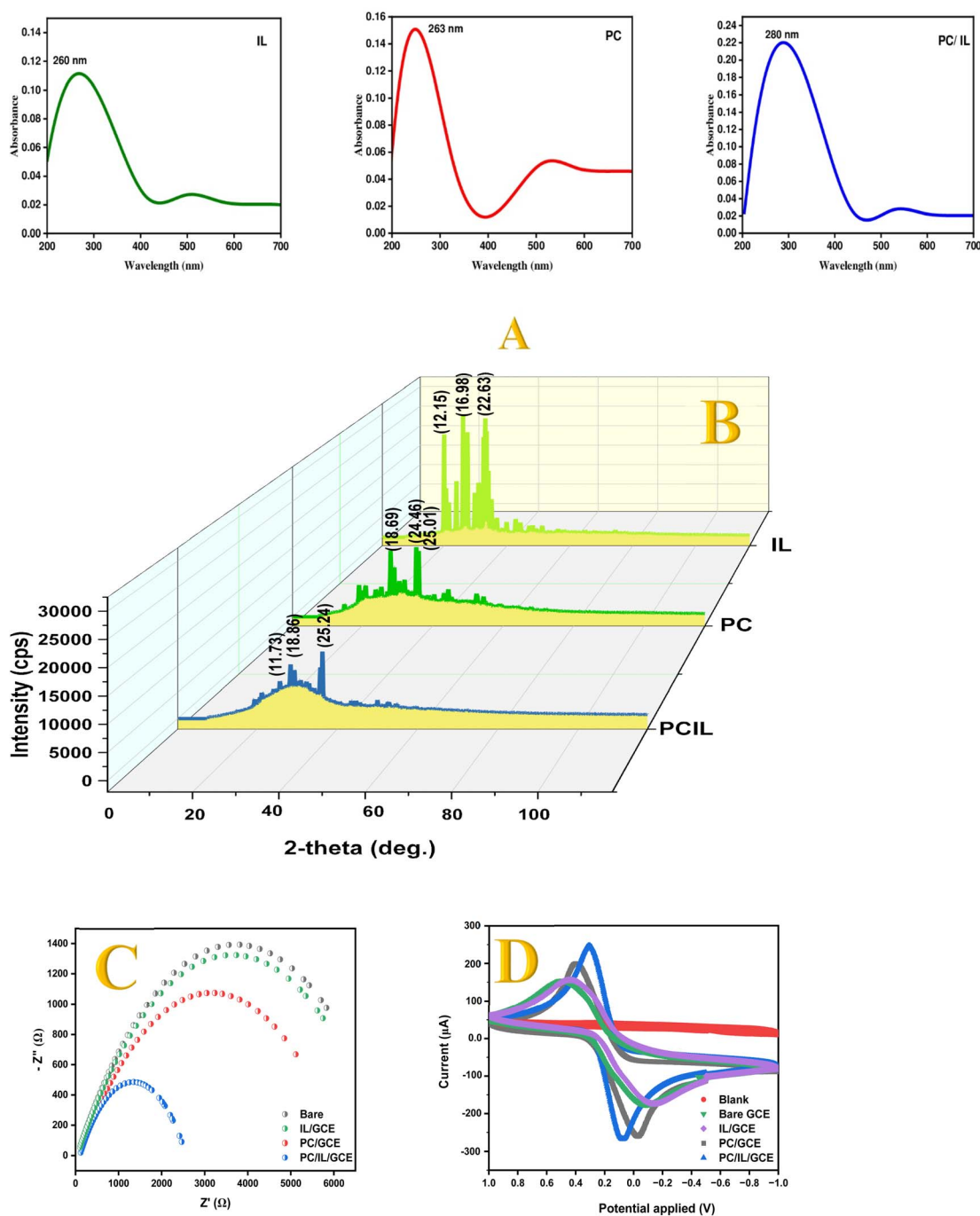


Fig. 2 (A) UV analysis of IL, PC and PC/IL; (B) XRD analysis of IL, PC and PC/IL; (C) EIS analysis of bare, IL, PC and PC/IL; (D) cyclic voltammograms of bare, IL, PC and PC/IL.

$\text{K}_3[\text{Fe}(\text{CN})_6]$, the value of D is $7.6 \times 10^{-6} \text{ cm}^2 \text{ s}^{-1}$ and n is 1. The effective surface areas (A) of bare GCE, PC@GCE, and PC/IL@GCE were calculated from the slope of the plot of I vs. $\nu^{1/2}$, which showed a linear relationship obtained by cyclic voltammetry. The effective electrode surface area for PC/IL@GCE was found to be 0.031 cm^2 , which was significantly greater than those of PC@GCE (0.026 cm^2), IL@GCE (0.021 cm^2) and bare GCE (0.018 cm^2). The electrocatalytic performance of PC@GCE was enhanced by addition of the ionic liquid, and the

developed PC/IL@GCE exhibited better electrochemical activity compared to PC@GCE and bare GCE.

3.4. Optimization of experimental conditions for the developed sensor

The cathodic current of TCP (80 ng mL^{-1}) decreases gradually with the increase in the pH of the Britton–Robinson (BR) buffer solution, as shown in ESI 3a.† Furthermore, with the increase in pH, the peak potential shifted toward the negative side. This

reveals that the pH of the supporting electrolyte exerted a significant influence on the electroreduction of TCP (ESI 3c,† indicating protonation during the electrode process). In acidic medium, H⁺ ions catalyze the reaction by making the carbonyl carbon more positive and thereby favour attack by the nucleophile and shift the equilibrium to the right direction.³⁴ The relationship between the reduction peak potential (E_p) and pH has been shown by a calibration plot between E_p and pH (ESI 3b†), which is expressed by eqn (iii) in the following:

$$E_p/V = -0.0373 \text{ pH} - 1.6141; (R^2 = 0.9932) \quad (\text{iii})$$

The effect of different volumes of the PC/IL hybrid composite on TCP reduction current at 80 ng mL⁻¹ was determined by the increasing volume of PC/IL suspension – cast onto the GCE surface. The change in TCP reduction current was recorded by changing the volume of different loading concentration (2–12 μL) of PC/IL suspension. ESI 4† shows that the peak current increases with the volume of PC/IL composite up to 10 μL and then decreases inversely due to the large background current. An extremely thin layer adsorbs less TCP, while an extra thick layer blocks the electrode surface, so an optimal concentration 10 μL was selected.

CV has been applied to study the redox behaviour of the TCP (ESI 5c†). For this purpose, electrocatalytic behaviour of TCP solution (80 ng mL⁻¹) was investigated in the potential range of 0.0 V to -2.5 V. One reduction peak was observed on initiating in the negative direction (0.0 to -2.5), and the absence of an anodic peak during the reverse scan (-2.5 to 0.0) pointed out that the process was irreversible. The influence of scan rate on the peak current and peak potential is presented in ESI 5.† It has been observed from ESI 5b† that the peak current increases linearly with increasing scan rate from 10 mV s⁻¹ to 100 mV s⁻¹, which also confirms that the reduction of TCP was diffusion controlled in the fabricated sensor, expressed by eqn (iv) as follows:

$$\text{TCP: } I(\mu\text{A}) = -12.8313\nu^{1/2} - 22.4322; (R^2 = 0.9912) \quad (\text{iv})$$

The effect of different SWV and DPV parameters, such as frequency, amplitude, and deposition potential, were also examined during the experiment. The influence of these parameters on cathodic peak current was optimized in a pre-experiment over the potential range 0.0 V to -2.0 V, and the results are depicted in ESI 6.† The modulation amplitude was increased from 10 to 200 mV, while other parameters were kept constant (modulation time, interval time and step potential), and a significant growth in peak was recorded up to 90 mV beyond which the peak deformed. The step potential was recorded in the range of 5–100 mV (with constant modulation time, modulation amplitude, and interval time), and 10 mV was recorded best with a stable and well-developed peak. As the interval time increases (10–100 ms, with constant modulation time, modulation amplitude, and step potential), an increase in current is recorded. Subsequently, 100 ms with the highest current is selected for further studies. The best scan window from -1.2 to -1.9 V for SWV and 0.0 to -2.0 V for DPV was

Table 1 Summary table for optimized parameters

| Operational parameters | Optimum value |
|---------------------------|---------------|
| Optimal pH | BR 1.78 |
| Fabrication concentration | 10 μL |
| Scan rate | 100 mV s |
| Solvent | Ethanol |
| Frequency | 70 Hz |
| Amplitude | 100 mV |
| Modulation amplitude | 90 mV |
| Modulation time | 40 ms |
| Step potential | 10 mV |
| Interval time | 100 ms |

selected to obtain sharp and defined peaks for TCP analysis using optimized parameters. The optimized condition showed that the developed sensor involves the electroreduction of TCP by protonation between the electrode surface and the analyte. An optimum concentration of fabrication helps to mediate the exchange of protons and enhance the electrocatalytic activity of the sensor; the optimized instrumental parameters are summarized in Table 1.

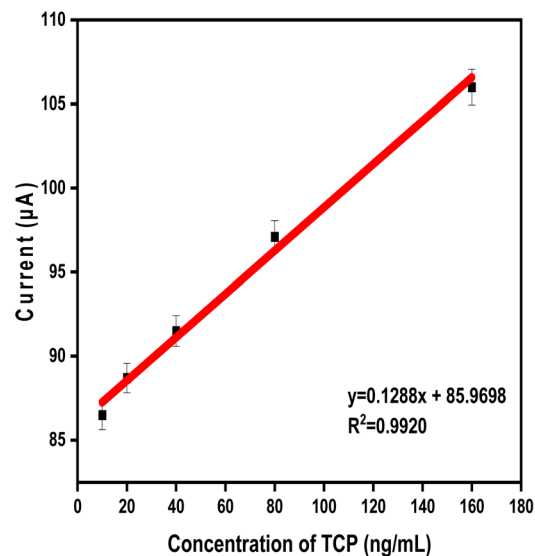
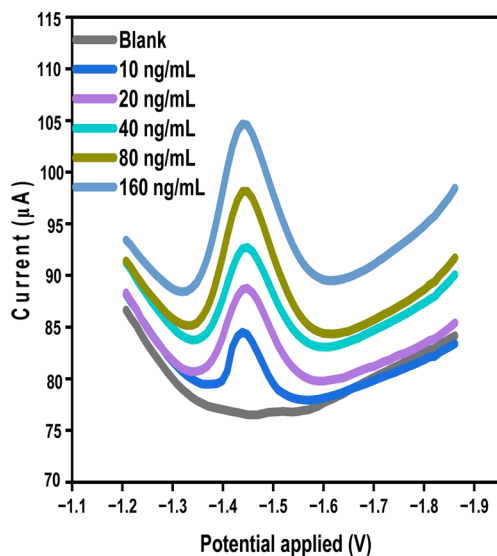
3.5. Electrochemical detection of TCP at PC/IL@GCE

The feasibility of the proposed method for quantifying TCP was established by examining the relationship between the reductive peak current and the concentration of the analyte using square wave voltammetry and differential pulse voltammetry at a PC/IL@GCE hybrid sensor. Under optimized conditions, voltammograms obtained with increasing amounts of TCP demonstrated that the peak current response increased linearly with increasing concentrations (Fig. 3). The calibration curve was linear over a wide concentration range, from 10 ng mL⁻¹ to 160 ng mL⁻¹ for a standard solution of TCP. The calibration plot resulted in a straight line, and the linear regression equation is given in eqn (v):

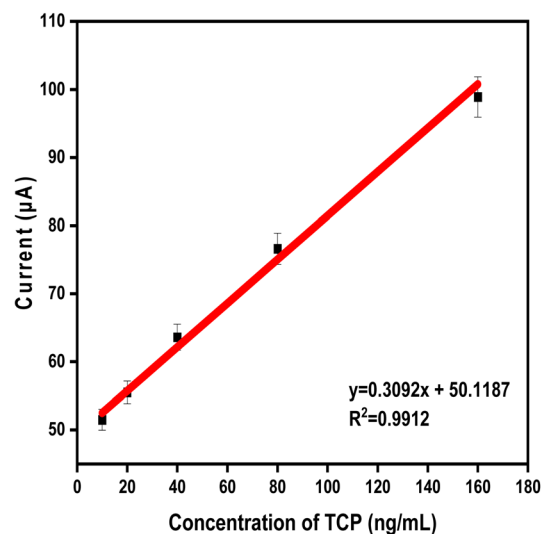
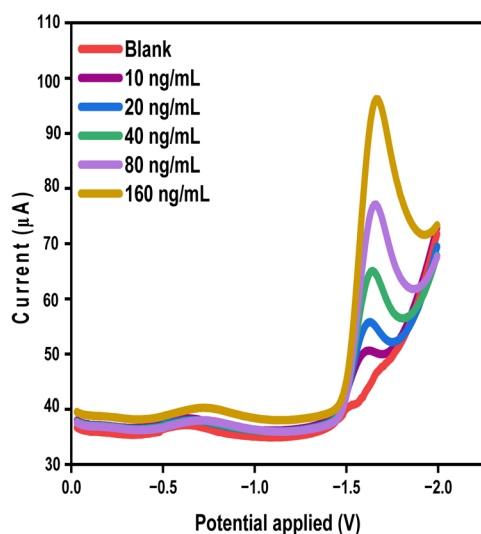
$$y = 0.1288x + 85.9698, R^2 = 0.9920 \text{ (SWV)} \quad (\text{v})$$

$$y = 0.3092x + 50.1187, R^2 = 0.9912 \text{ (DPV)} \quad (\text{vi})$$

The observed limit of detection (LOD) and limit of quantification (LOQ) *via* SWV and DPV for standard solution were 586 pg mL⁻¹ and 1.953 ng mL⁻¹ and 223 pg mL⁻¹ and 745 pg mL⁻¹, respectively. After standardization of the developed method, comparative results were obtained for the real samples (ESI 7†). Comparative LOD and LOQ for tomato, apple, and human serum are illustrated in Table 2. From Table 2, it is seen that due to the sample matrix effect, the performance of the sensor is influenced, and the LOD and LOQ values of real samples are somewhat enhanced than the standard solution. Furthermore, the determination parameters of TCP using this method were compared with those of other electroanalytical sensors, and the results are listed in Table 3. The data in Table 3 indicate that the developed method is applicable, sensitive and comparable over a wider concentration range and provides a lower LOD. After



(A)



(B)

Fig. 3 Calibration curve of standard solution for TCP reduction at concentrations from 10 to 160 ng mL^{-1} : (A) SWV and (B) DPV.

evaluating the sensitivity of the same sensor with two comparative methods, DPV was found to be more sensitive than SWV, and the developed sensor was found to be robust with two different applied methods.

3.6. Reproducibility, stability and interference studies

The fabricated PC/IL@GCE showed highly reproducible electrochemical performance toward the detection of TCP (80 ng mL^{-1}). For this, three different electrode sensors were fabricated, and their reproducibility toward TCP was evaluated using DPV at different times (ST 2). The reliability of the developed sensor depends on the relative standard deviation (RSD) in the

Table 2 Calibration range, LOD and LOQ of standard and different real samples

| Samples | SWV | | | DPV | | |
|-------------------|---------------------------|----------------------------|-------------------------------------|---------------------------|---------------------------|-------------------------------------|
| | LOD | LOQ | LDR (R^2) | LOD | LOQ | LDR (R^2) |
| Standard solution | 0.586 ng mL ⁻¹ | 1.953 ng mL ⁻¹ | 10–160 ng mL ⁻¹ (0.9920) | 0.223 ng mL ⁻¹ | 0.745 ng mL ⁻¹ | 10–160 ng mL ⁻¹ (0.9912) |
| Human serum | 3.973 ng mL ⁻¹ | 13.243 ng mL ⁻¹ | 10–160 ng mL ⁻¹ (0.9945) | 1.025 ng mL ⁻¹ | 3.419 ng mL ⁻¹ | 10–160 ng mL ⁻¹ (0.9901) |
| Tomato | 1.992 ng mL ⁻¹ | 6.640 ng mL ⁻¹ | 10–160 ng mL ⁻¹ (0.9935) | 0.981 ng mL ⁻¹ | 3.272 ng mL ⁻¹ | 10–160 ng mL ⁻¹ (0.9914) |
| Apple | 2.094 ng mL ⁻¹ | 6.980 ng mL ⁻¹ | 10–160 ng mL ⁻¹ (0.9912) | 0.948 ng mL ⁻¹ | 3.162 ng mL ⁻¹ | 10–160 ng mL ⁻¹ (0.9913) |

Table 3 Comparison of the limit of detection of the proposed method with earlier reported methods

| Technique | pH | Sensor | LOD (ng mL ⁻¹) | Solvent | Real sample | Reference |
|-------------------------------|------|---|----------------------------|-----------------------|--|------------|
| Immunoaffinity chromatography | 7.2 | Immunoaffinity column | — | Ethanol/water | Water | 7 |
| SWV | 2 | Boron-doped diamond | 474 | Acetonitrile | Water and urine | 11 |
| DPV | — | — | 210 | — | — | — |
| ^a UV-MALDI-MS | — | Laser | 2.00 | — | Soil | 35 |
| SWV | 2.5 | ^a PANI/C70/GCE | 1.90 | TritonX-100 | Tomato | 10 |
| Surface plasmon resonance | — | Gold nanorods | 1.03 × 10 ³ | — | — | 9 |
| Photoelectro-Fenton | 7 | Boron-doped diamond anode | 1.54 × 10 ⁴ | Chlorine | — | 36 |
| Fluorescence | — | <i>n</i> -Butyl-1,8-naphthalimide Schiff base | 74.1 | DMSO–H ₂ O | Wheat seedlings, sugarcane, broadleaf weed and water samples | 8 |
| DPV | 1.78 | PC/IL@GCE | 0.22 | Ethanol | Tomato, apple and human serum | This study |
| SWV | — | — | 0.59 | — | — | — |

^a Chemiluminescence enzyme-linked immunosorbent assay (CL-ELISA). Ultraviolet matrix-assisted laser desorption/ionization mass spectrometry (UV-MALDI-MS). Polyaniline (PANI). Liquid chromatography mass spectrometry (LC-MS).

cathodic peak current obtained by three replicates of different sensors. The sensor response was less than 1.5% of RSD, suggesting their high sensitivity toward electrochemical applications.

The stability of the sensor was further assessed using DPV to measure a consistent concentration of TCP (80 ng mL⁻¹) over the course of one month, with measurements taken weekly. The sensor was stored in a desiccator at 25 °C without sunlight, and after two weeks the sensor retained 85% of its initial response to TCP, demonstrating the high stability of the PC/IL@GCE sensor. Moreover, the anti-interference ability of the sensor toward TCP was studied in the presence of other organic and inorganic interferents such as *L*-tryptophan, tartaric acid, *L*-aspartic acid, citric acid, KCL, NaCl, and MgSO₄ (Fig. 4A). The study showed good specificity of the developed sensor toward TCP reduction among these interferents, suggesting that the fabricated sensor is rapid and specific for the detection of the analyte (ST 3). TCP determination was carried out in acidic medium (BR 1.78), that also accelerate the oxidation of the organic interferent and does not interfere with the reduction process of TCP. Increased concentrations of interferent showed no further change in the peak current, suggesting the specificity of peak potential towards TCP reduction in the matrices.

The selectivity of the electrode for TCP was also tested in the presence of similar structure compounds like alachlor, urea, and sodium azide (ST 4). Active binding sites of PC/IL@GCE

selectively bind with trichlopyr due to electrostatic interactions, and acidic medium accelerates its interaction with the sensor surface, as compared with other similar structured compounds. The study showed no obvious change in the peak current or peak potential toward TCP reduction, suggesting high selectivity of the sensor toward the analyte in the presence of agents having a similar structure (Fig. 4B).

3.7. Recovery studies

The analytical utility of the developed sensor was justified by its application in the detection of TCP in synthetic serum and fruits. For the analysis, the solution was obtained by the addition of an adequate amount of TCP in a previously prepared stock solution of each real sample. The SWV and DPV current responses with acceptable recoveries between 99.64–101.92%, 99.44–100.87%, and 99.02–101.40% were obtained using the standard addition method for the detection of TCP in real samples of serum, tomato, and apple, respectively. The corresponding results have been shown in ST 5, clearly demonstrating the successful application of the developed sensor for the determination of TCP in real samples.

3.8. Kinetics of reaction

Langmuir and Freundlich isotherms were applied to understand the binding chemistry between analyte molecules and the fabricated sensor.³⁷ Langmuir isotherms suggest monolayer

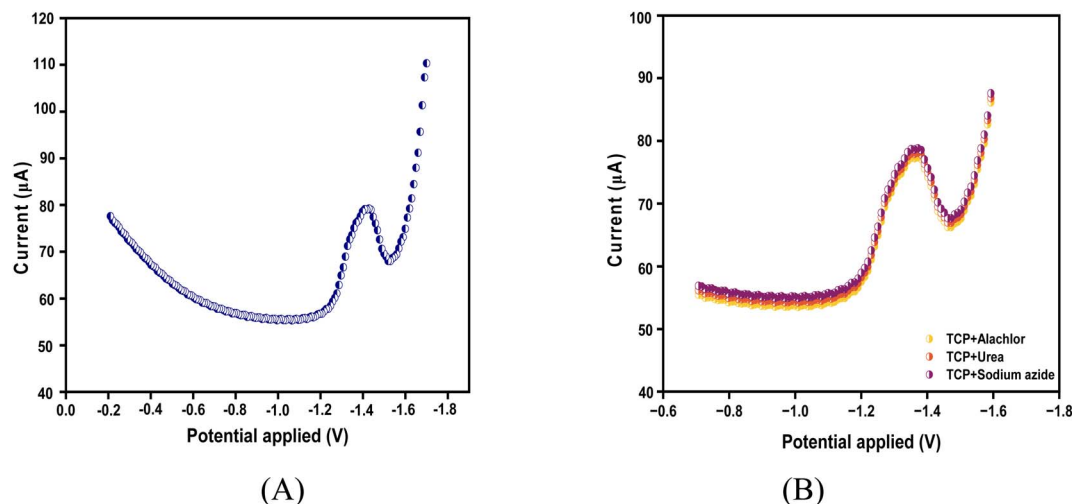


Fig. 4 (A) DPV curve showing reduction of TCP in the presence of interferents: L-tryptophan, tartaric acid, L-aspartic acid, citric acid, KCl, NaCl, and MgSO_4 ; (B) DPV curve showing reduction of TCP in the presence of similar structure compounds: alachlor, urea, and sodium azide.

contact with uniformly distributed binding sites and no lateral interactions,³⁸ whereas the Freundlich isotherms indicate multilayer interaction between the analyte and binding site heterogeneity.³⁹ These models are employed for sensor data processing with certain mathematical modifications, even though they are hypothesized for the gas adsorption process.⁴⁰ For such models, the following modified linear formula was applied:

$$\text{Langmuir: } \Delta I = (\Delta I_{\text{max}} C / K_D + C) \quad (\text{vii})$$

$$\text{Freundlich: } \Delta I = \Delta I_{\text{max}} C^{1/n} \quad (\text{viii})$$

Herein, ΔI , ΔI_{max} , C , K_D , and $1/n$ designate the actual current shift (μA), theoretical maximum current shift (μA), analyte concentration (M), equilibrium constant, and Freundlich coefficient, respectively.

The regression coefficients (R^2) for each (DPV and SWV) of these models are high for the Freundlich isotherm when applied to the concentration vs. current (ESI 8†) data of the calibration curve. The value of n represents the heterogeneous binding sites of IL when combined with pectin that enhance the multilayer interaction of analyte molecules with binding sites and accelerate the catalytic activity of TCP. The analyzed data have been shown in ST 6. A greater value of ΔI_{max} in the Freundlich isotherm represents greater current shift, which accelerates the interaction of the analyte at the electrode surface.⁴¹

4. Greenness of the PC/IL@GCE sensor

The greenness of any methods of analysis is a complex, diverse measurement that is difficult to measure.⁴² The idea of “green analytical chemistry” (GAC) forces analytical chemists to ensure that the safety, health, and the environment are taken into

account when working.⁴³ It is evident that GAC needs specific numbers to evaluate whether the environmentally conscious analytical techniques are a green method of analysis or not. Software that is freely available simplifies the evaluation process. AGREE is a free software and can be accessed at <https://mostwiedzy.pl/AGREE>.⁴⁴ It evaluates the greenness of processes using the GAC principles, ESI 10.† According to the GAC principles, *in situ* sample preparation, placement (portable device), their measurements and less use of hazardous materials provide high weightage to GAC principles. All the GAC principles supported the greenness of the developed method with a good score.⁴⁴ So the developed method is found to be more greener in comparison with other conventional methods,^{7–11,35,36} because natural materials were used for the sensor preparation along with the use of green solvents, the portable device shifts the method towards enhanced greenness, less waste generation, less energy consumption, and use of more sustainable and renewable materials, all these made this method more greener and significantly high scoring.

One of the most notable benefits of this process is that it eliminates the preparative stage, which is arduous, time-consuming, and requires a considerable volume of dangerous organic solvents. In contrast to our research, the majority of electrochemical analysis procedures involve non-green chemicals, reagents, and methods. Previously reported electrochemical methods for PANI/C70/GCE¹⁰ and BDD⁹ are not green and less sensitive than the developed method. The greenness and environmental friendliness of the developed approach could be assessed when it was compared in terms of electrode components.⁴⁵ The score and weight list criteria for this electrochemical analysis method (ESI 9†) demonstrate the 92% greener aspect of the developed method.

5. Conclusion

In this study, an electrochemical sensor based on a pectin and ionic liquid composite has been developed for the first time, to the best of our knowledge. The sensor exhibited several unique characteristics, including a high electroactive surface area, interconnecting porous channels, and excellent electrical conductivity. It was then employed for the electrochemical detection of triclopyr, a herbicide used for controlling broadleaf weeds and woody plants. The proposed method was found to be superior to previously reported electroanalytical methods for TCP detection.^{10,11} The developed sensor based on green material demonstrated high sensitivity, a low detection limit, good reproducibility, and stability in TCP analysis. Recovery studies using real samples of human serum, tomatoes, and apples showed that the sensor provided rapid and sensitive detection of TCP. The novelty of this work lies in the use of PC/IL@GCE as a green material-based sensor for TCP detection, making it a promising material for future sensing applications due to its environment-friendly properties, excellent electrochemical performance, high electroactive surface area and cost-effectiveness. However, with these advancements, the developed electrode also has limitations. Pectin is a biopolymer, and it is not easy to stabilize it over the electrode surface for a long time. In the case of humid atmosphere, the ionic liquid absorbs moisture and resists adherence to the electrode surface and may prove challenging. Due to short shelf life of the electrode its maintenance is a challenging task. In future, lab-on-chip devices can be made, which may overcome these limitations and can be used for on-site analysis.

Data availability

The data supporting this article have been included as part of the ESI.† The developed green sensor significantly showed lower limits, and its greenness was determined with AGREE software. It is free software and can be accessed at <https://mostwiedzy.pl/AGREE>.

Author contributions

Puja Tomar: investigation, data analysis, writing – original draft. Nimisha Jadon: conceptualization, methodology, supervision, validation, review & editing. Swati Shrivastava: data analysis, validation, writing – review & editing.

Conflicts of interest

The authors declare no conflict of interest, financial or otherwise.

Acknowledgements

The authors extend their gratitude to the Central Instrumentation Facility, Jiwaji University, India, and University Sophisticated Instrument Facility, Aligarh Muslim University, India for providing assistance in the characterization of the material and

School of Studies in Environmental Science for providing lab facility to conduct this study.

References

- 1 U. EPA Office of Pesticide Programs, *US EPA – Pesticides – Fact Sheet for Triclopyr*, 1998.
- 2 M. Bartels, C. Brown, G. Chung, M. Chan, C. Terry, S. Gehen and M. Corvaro, Review of the pharmacokinetics and metabolism of triclopyr herbicide in mammals: impact on safety assessments, *Regul. Toxicol. Pharmacol.*, 2020, **116**, 104714, DOI: [10.1016/j.yrtph.2020.104714](https://doi.org/10.1016/j.yrtph.2020.104714).
- 3 A. J. Cessna, R. Grover and D. T. Waite, Environmental fate of triclopyr, *Rev. Environ. Contam. Toxicol.*, 2002, **174**, 19–48, DOI: [10.1007/978-1-4757-4260-2](https://doi.org/10.1007/978-1-4757-4260-2).
- 4 M. Tu, C. Hurd, J. M. Randall and B. Rice, *Weed Control Methods Handbook*, The Nature Conservancy, 2001, <http://tncweeds.ucdavis.edu/version>.
- 5 Diario Oficial de las Comunidades Europeas ES.
- 6 EPA-HQ-OPP-2014-0576-0035_content.
- 7 F. G. Sanchez, A. N. Diaz, R. G. Herrera and L. P. San Jose, Development and characterisation of an immunoaffinity chromatographic column for the on-line determination of the pesticide triclopyr, *Talanta*, 2007, **71**, 1411–1416, DOI: [10.1016/j.talanta.2006.07.015](https://doi.org/10.1016/j.talanta.2006.07.015).
- 8 Y. Li, J. Guo, L. Lin, H. Guo and F. Yang, A color-changed fluorescence sensor for pesticide triclopyr 2-butoxyethyl ester based on naphthalimide Schiff-base, *J. Photochem. Photobiol., A*, 2024, **457**, 115894, DOI: [10.1016/j.jphotochem.2024.115894](https://doi.org/10.1016/j.jphotochem.2024.115894).
- 9 N. Z. An'Nisa, M. Morsin, R. Sanudin, N. L. Razali and S. Nafisah, Controlled wet chemical synthesis of gold nanorods for triclopyr butotyl herbicide detection based-plasmonic sensor, *Sens Biosensing Res.*, 2020, **29**, 100359, DOI: [10.1016/j.sbsr.2020.100359](https://doi.org/10.1016/j.sbsr.2020.100359).
- 10 A. Pandey, S. Sharma and R. Jain, Voltammetric sensor for the monitoring of hazardous herbicide triclopyr (TCP), *J. Hazard. Mater.*, 2019, **367**, 246–255, DOI: [10.1016/j.jhazmat.2018.12.083](https://doi.org/10.1016/j.jhazmat.2018.12.083).
- 11 L. Janikova-Bandzuchova, R. Šeššová, K. Schwarzová-Pecková and J. Chýlková, Sensitive voltammetric method for rapid determination of pyridine herbicide triclopyr on bare boron-doped diamond electrode, *Electrochim. Acta*, 2015, **154**, 421–429, DOI: [10.1016/j.electacta.2014.12.064](https://doi.org/10.1016/j.electacta.2014.12.064).
- 12 A. Dube, S. J. Malode, M. Ali Alshehri and N. P. Shetti, Recent advances in the development of electrochemical sensors for detecting pesticides, *J. Ind. Eng. Chem.*, 2024, **144**, 77–99, DOI: [10.1016/j.jiec.2024.09.042](https://doi.org/10.1016/j.jiec.2024.09.042).
- 13 N. Jadon, A. Pandey and H. K. Sharma, Selective and sensitive PANI-CeO₂ coated gold sensor for electrocatalytic sensing of hypersensitive drugs, *Sens Biosensing Res.*, 2019, **22**, 100256, DOI: [10.1016/j.sbsr.2019.100256](https://doi.org/10.1016/j.sbsr.2019.100256).
- 14 N. Jadon and H. K. Sharma, PANI/Chitosan/Ionic Liquid/GCE Sensor for the Selective Quantification of Domperidone (DMP) and Pantoprazole (PTZ), *Anal. Chem. Lett.*, 2020, **10**, 537–549, DOI: [10.1080/22297928.2020.1837668](https://doi.org/10.1080/22297928.2020.1837668).

- 15 S. Shrivastava, N. Jadon and R. Jain, Next-generation polymer nanocomposite-based electrochemical sensors and biosensors: A review, *TrAC, Trends Anal. Chem.*, 2016, **82**, 55–67, DOI: [10.1016/j.trac.2016.04.005](https://doi.org/10.1016/j.trac.2016.04.005).
- 16 N. Jadon, R. Jain and A. Pandey, Electrochemical analysis of amlodipine in some pharmaceutical formulations and biological fluid using disposable pencil graphite electrode, *J. Electroanal. Chem.*, 2017, **788**, 7–13, DOI: [10.1016/j.jelechem.2017.01.055](https://doi.org/10.1016/j.jelechem.2017.01.055).
- 17 K. Radhapyari, S. Datta, S. Dutta, N. Jadon and R. Khan, Graphene-based nanostructures for biomedical applications, in *Two-Dimensional Nanostructures for Biomedical Technology: A Bridge between Material Science and Bioengineering*, 2019, pp. 101–135, DOI: [10.1016/B978-0-12-817650-4.00004-8](https://doi.org/10.1016/B978-0-12-817650-4.00004-8).
- 18 Y. Zheng, C. Yu and L. Fu, Biochar-based materials for electroanalytical applications: an overview, *Green Anal. Chem.*, 2023, **7**, 100081, DOI: [10.1016/j.greac.2023.100081](https://doi.org/10.1016/j.greac.2023.100081).
- 19 S. I. Kaya, G. Ozcelikay-Akyildiz and S. A. Ozkan, Green metrics and green analytical applications: A comprehensive outlook from developing countries to advanced applications, *Green Anal. Chem.*, 2024, **11**, 100159, DOI: [10.1016/j.greac.2024.100159](https://doi.org/10.1016/j.greac.2024.100159).
- 20 L. Shi and S. Gunasekaran, Preparation of pectin-ZnO nanocomposite, *Nanoscale Res. Lett.*, 2008, **3**, 479, DOI: [10.1007/s11671-008-9185-6](https://doi.org/10.1007/s11671-008-9185-6).
- 21 H. Jonassen, A. Treves, A. L. Kjøniksen, G. Smistad and M. Hiorth, Preparation of ionically cross-linked pectin nanoparticles in the presence of chlorides of divalent and monovalent cations, *Biomacromolecules*, 2013, **14**, 3523–3531, DOI: [10.1021/bm4008474](https://doi.org/10.1021/bm4008474).
- 22 N. Krithiga, K. B. Viswanath, V. S. Vasantha and A. Jayachitra, Specific and selective electrochemical immunoassay for *Pseudomonas aeruginosa* based on pectin-gold nano composite, *Biosens. Bioelectron.*, 2016, **79**, 121–129, DOI: [10.1016/j.bios.2015.12.006](https://doi.org/10.1016/j.bios.2015.12.006).
- 23 M. Vasudevan, V. Perumal, S. Karuppanan, M. Ovinis, P. Bothi Raja, S. C. B. Gopinath and T. N. J. Immanuel Edison, A Comprehensive Review on Biopolymer Mediated Nanomaterial Composites and Their Applications in Electrochemical Sensors, *Crit. Rev. Anal. Chem.*, 2022, 1871–1894, DOI: [10.1080/10408347.2022.2135090](https://doi.org/10.1080/10408347.2022.2135090).
- 24 E. F. Fiorentini, M. Llaver, M. N. Oviedo, P. Y. Quintas and R. G. Wuilloud, State-of-the-art analytical methods based on ionic liquids for food and beverage analysis, *Green Anal. Chem.*, 2022, **1**, 100002, DOI: [10.1016/j.greac.2022.100002](https://doi.org/10.1016/j.greac.2022.100002).
- 25 A. Cetinkaya, S. I. Kaya, M. Yence, F. Budak and S. A. Ozkan, Ionic liquid-based materials for electrochemical sensor applications in environmental samples, *Trends Environ. Anal. Chem.*, 2023, **37**, e00188, DOI: [10.1016/j.teac.2022.e00188](https://doi.org/10.1016/j.teac.2022.e00188).
- 26 F. Endres, Physical chemistry of ionic liquids, *Phys. Chem. Chem. Phys.*, 2010, **12**, 1648, DOI: [10.1039/c001176m](https://doi.org/10.1039/c001176m).
- 27 A. Abo-Hamad, M. A. Alsaadi, M. Hayyan, I. Juneidi and M. A. Hashim, Ionic Liquid-Carbon Nanomaterial Hybrids for Electrochemical Sensor Applications: A Review, *Electrochim. Acta*, 2016, **193**, 321–343, DOI: [10.1016/j.electacta.2016.02.044](https://doi.org/10.1016/j.electacta.2016.02.044).
- 28 K. Arya and B. Prabhakar, Ionic liquid confined zeolite system: An approach towards water mediated room temperature synthesis of spiro[pyrazolo[3,4-e]benzothiazepines], *Green Chem.*, 2013, **15**, 2885–2894, DOI: [10.1039/c3gc40553b](https://doi.org/10.1039/c3gc40553b).
- 29 S. P. Ho, S. C. Yeong, M. J. Young and H. H. Won, Intermolecular interaction-induced hierarchical transformation in 1D nanohybrids: Analysis of conformational changes by 2D correlation spectroscopy, *J. Am. Chem. Soc.*, 2008, **130**(3), 845–852, DOI: [10.1021/ja073074k](https://doi.org/10.1021/ja073074k).
- 30 F. P. Kinik, A. Uzun and S. Keskin, Ionic Liquid/Metal–Organic Framework Composites: From Synthesis to Applications, *ChemSusChem*, 2017, **10**, 2842–2863, DOI: [10.1002/cssc.201700716](https://doi.org/10.1002/cssc.201700716).
- 31 M. Bakhtiarian and M. M. Khodaei, Pyridinium-based dual acidic ionic liquid supported on the pectin for efficient synthesis of pyrazoles, *J. Mol. Liq.*, 2022, **363**, 119883, DOI: [10.1016/j.molliq.2022.119883](https://doi.org/10.1016/j.molliq.2022.119883).
- 32 M. L. Fishman, H. K. Chau, P. X. Qi, A. T. Hotchkiss, R. A. Garcia and P. H. Cooke, Characterization of the global structure of low methoxyl pectin in solution, *Food Hydrocolloids*, 2015, **46**, 153–159, DOI: [10.1016/j.foodhyd.2014.12.021](https://doi.org/10.1016/j.foodhyd.2014.12.021).
- 33 K. D. Hari, C. V. Garcia, G. H. Shin and J. T. Kim, Improvement of the UV barrier and antibacterial properties of crosslinked pectin/zinc oxide bionanocomposite films, *Polymers*, 2021, **13**, 2403, DOI: [10.3390/polym13152403](https://doi.org/10.3390/polym13152403).
- 34 J. March, *Advanced Organic Chemistry : Reactions, Mechanisms, and Structure*, Wiley, 4th edn, 1992.
- 35 B. Ivanova, Solid-state UV-MALDI mass spectrometric quantitation of fluroxypyr and triclopyr in soil, *Environ. Geochem. Health*, 2015, **37**, 557–574, DOI: [10.1007/s10653-014-9673-9](https://doi.org/10.1007/s10653-014-9673-9).
- 36 I. C. Da Costa Soares, R. Oriol, Z. Ye, C. A. Martínez-Huitle, P. L. Cabot, E. Brillas and I. Sirés, Photoelectro-Fenton treatment of pesticide triclopyr at neutral pH using Fe(III)–EDDS under UVA light or sunlight, *Environ. Sci. Pollut. Res.*, 2021, **28**, 23833–23848, DOI: [10.1007/s11356-020-11421-8](https://doi.org/10.1007/s11356-020-11421-8).
- 37 L. Uzun, R. Say, S. Ünal and A. Denizli, Production of surface plasmon resonance based assay kit for hepatitis diagnosis, *Biosens. Bioelectron.*, 2009, **24**, 2878–2884, DOI: [10.1016/j.bios.2009.02.021](https://doi.org/10.1016/j.bios.2009.02.021).
- 38 X. Li and S. M. Husson, Adsorption of dansylated amino acids on molecularly imprinted surfaces: A surface plasmon resonance study, *Biosens. Bioelectron.*, 2006, **22**, 336–348, DOI: [10.1016/j.bios.2006.04.016](https://doi.org/10.1016/j.bios.2006.04.016).
- 39 R. J. Umpleby, S. C. Baxter, Y. Chen, R. N. Shah and K. D. Shimizu, Characterization of molecularly imprinted polymers with the Langmuir - Freundlich isotherm, *Anal. Chem.*, 2001, **73**, 4584–4591, DOI: [10.1021/ac0105686](https://doi.org/10.1021/ac0105686).
- 40 T. Karasu, N. İdil, E. Özgür and L. Uzun, *Pseudomonas aeruginosa* imprinted polydopamine@graphene-coated

- pencil graphite electrode for selective bacterial detection, *Colloids Surf., A*, 2024, **681**, 132788, DOI: [10.1016/j.colsurfa.2023.132788](https://doi.org/10.1016/j.colsurfa.2023.132788).
- 41 N. A. Manrique Rodriguez, M. Costa, S. Di Masi, C. Zaleski, A. Garcia-Cruz, G. Mele, V. M. Paradiso, S. Piletsky, C. Malitesta and G. E. De Benedetto, Adsorption Isotherm Analysis for Hybrid Molecularly Imprinted Polymeric Gold-Decorated Nanoparticles Suitable for Reliable Quantification of Gluconic Acid in Wine, *Nanomaterials*, 2025, **15**, 211, DOI: [10.3390/nano15030211](https://doi.org/10.3390/nano15030211).
- 42 M. Tobiszewski, M. Marć, A. Gałuszka and J. Namieśnik, Green chemistry metrics with special reference to green analytical chemistry, *Molecules*, 2015, **20**, 10928–10946, DOI: [10.3390/molecules200610928](https://doi.org/10.3390/molecules200610928).
- 43 S. Armenta, S. Garrigues and M. de la Guardia, Green Analytical Chemistry, *TrAC, Trends Anal. Chem.*, 2008, **27**, 497–511, DOI: [10.1016/j.trac.2008.05.003](https://doi.org/10.1016/j.trac.2008.05.003).
- 44 F. Pena-Pereira, W. Wojnowski and M. Tobiszewski, AGREE – Analytical GREENness Metric Approach and Software, *Anal. Chem.*, 2020, **92**, 10076–10082, DOI: [10.1021/acs.analchem.0c01887](https://doi.org/10.1021/acs.analchem.0c01887).
- 45 A. Cetinkaya, E. Yıldız, S. I. Kaya, M. E. Çorman, L. Uzun and S. A. Ozkan, A green synthesis route to develop molecularly imprinted electrochemical sensor for selective detection of vancomycin from aqueous and serum samples, *Green Anal. Chem.*, 2022, **2**, 100017, DOI: [10.1016/j.greeac.2022.100017](https://doi.org/10.1016/j.greeac.2022.100017).